Computers in Biology and Medicine 179 (2024) 108828

Contents lists available at ScienceDirect

Computers in Biology and Medicine

journal homepage: www.elsevier.com/locate/compbiomed

The relation between aortic morphology and transcatheter aortic heart valve thrombosis: Particle tracing and platelet activation in larger aortic roots with and without neo-sinus

Karoline-Marie Bornemann *, Silje Ekroll Jahren, Dominik Obrist

ARTORG Center for Biomedical Engineering Research, University of Bern, Freiburgstrasse 3, Bern, 3010, Switzerland

ARTICLE INFO

Keywords:
Computational modeling
Sinus washout
Fluid–structure interaction
Blood damage index
Shear stress
Direct Numerical Simulation
Flow stagnation

ABSTRACT

Transcatheter aortic heart valve thrombosis (THVT) affects long-term valve durability, transvalvular pressure gradient and leaflet mobility. In this study, we conduct high-fidelity fluid–structure interaction simulations to perform Lagrangian particle tracing in a generic model with larger aortic diameters (THVT model) with and without neo-sinus which is compared to a model of unaffected TAVI patients (control model). Platelet activation indices are computed for each particle to assess the risk of thrombus formation induced by high shear stresses followed by flow stagnation. Particle tracing indicates that fewer particles contribute to sinus washout of the THVT model with and without neo-sinus compared to the control model (−34.9%/−34.1%). Stagnating particles in the native sinus of the THVT model show higher platelet activation indices than for the control model (+39.6% without neo-sinus, +45.3% with neo-sinus). Highest activation indices are present for particles stagnating in the neo-sinus of the larger aorta representing THVT patients (+80.2% compared to control).

This fluid–structure interaction (FSI) study suggests that larger aortas lead to less efficient sinus washout in combination with higher risk of platelet activation among stagnating particles, especially within the neo-sinus. This could explain (a) a higher occurrence of thrombus formation in transcatheter valves compared to surgical valves without neo-sinus and (b) the neo-sinus as the prevalent region for thrombi in TAV. Pre-procedural identification of larger aortic roots could contribute to better risk assessment of patients and improved selection of a patient-specific anti-coagulation therapy.

1. Introduction

Transcatheter aortic valve implantation (TAV) presents a minimally invasive solution for patients at high surgical risk with moderate to severe aortic valve stenosis. As the leaflets are composed of biological material, mechanisms causing structural valve deterioration (SVD) such as leaflet calcification or tearing are considered relevant valve failure modes. Also, TAVI patients are prone to non-SVD processes such as patient-prosthesis mismatch and valve thrombosis [1]. Although anti-coagulation therapy after TAVI targets the prevention of such thrombus formation, transcatheter heart valve thrombosis (THVT) might be detected in routine follow-up [2]. The incidence of clinical THVT is rather low with percentages below 3% [3–5]. The incidental finding of subclinical THVT, however, is much more common, although its detection is strongly dependent on imaging techniques, diagnostic criteria and screening intensities (incidence 7% to 35% [2,6–9]).

Main contributing factors for the development of thrombosis are described in Virchow's triad connecting blood flow stasis, endothelial injury and hypercoagulability [10]. TAVIs significantly alter the flow field in the aortic root and the ascending aorta (AAo) as the sinus is divided into the reduced native sinus and a neo-sinus between stent, native leaflets and prosthetic valve leaflets [10]. Longer residence time of blood flow within the sinus and increased flow stasis in the neo-sinus, which is dependent on TAVI position [11,12], cardiac output [13] and volumetric size of the sinus portions [14], facilitate thrombus formation. The possibly resulting thin layer of thrombus on the aortic side of the prosthetic leaflets is then most commonly detected as hypoattenuating leaflet thickening (HALT) using multi-detector computed tomography (MDCT) [6,15–18]. If the thickening of the leaflets limits the leaflet motion by more than 50%, the patient is diagnosed with hypoattenuation affecting motion (HAM) [2].

High shear stresses in the systolic turbulent flow field in the ascending aorta (AAo) are associated with possible platelet activation [19,20]. The turbulent flow in the AAo was studied experimentally for

* Corresponding author.
E-mail address: karoline-marie.bornemann@unibe.ch (K.-M. Bornemann).

https://doi.org/10.1016/j.compbiomed.2024.108828
Received 27 March 2024; Received in revised form 5 June 2024; Accepted 29 June 2024
Available online 11 July 2024

Table 1
Aortic dimensions with sinotubular junction diameter d_{STJ} and ascending aorta diameter d_{AAo} relative to the annulus diameter (d_A = 22 mm) for control and THVT group.

	Control	THVT
d_A	22mm	
d_{STJ}	$1.15d_A$	$1.25d_A$
d_{AAo}	$1.3d_A$	$1.5d_A$

transcatheter aortic valves (TAV) by Pietrasanta et al. [12] using tomographic particle imaging velocimetry (Tomo-PIV). According to this study, implantation position is of significant relevance as lower implantation position causes higher turbulent kinetic energy and a narrower and faster core jet of the mean flow field which affects backflow patterns and therefore the transport to and the washout of the sinus portions. General sources for an efficient sinus washout were shown to be the aortic jet issuing from the TAV as well as the transient geometrical change of the neo-sinus due to leaflet motion [21,22]. Moreover, coronary flow was found to increase the sinus washout rate [13,23]. Singh-Gryzbon et al. [24] found a linear relation between thrombus and stasis volume using Computational Fluid Dynamics (CFD) to study patient anatomies of the aortic root. Combining segmented patient-specific computed tomography (CT) images and CFD, Hatoum et al. [21] presented a predictive mathematical model to assess thrombosis risk.

Aortic root morphology has been considered relevant for the development of thrombosis due to altered flow patterns and sinus washout [22,25–27]. Adverse events after TAVI (e.g. paravalvular regurgitation (PVR), increased risk of mortality, major bleeding in short- and long-term periods after surgery) were connected to aortic dilatation at the sinus of Valsalva [28]. However, the relation between aortic root morphology and the development of THVT seems to remain largely unknown. In our previous study [29], we investigated pre-surgical MDCT images of TAVI patients from the Bern TAVI registry and observed a larger AAo diameter in TAVI patients who developed THVT compared to unaffected TAVI patients. Further, we performed comparative fluid–structure interaction simulations evaluating the mean flow features in a normal and larger aorta. In the aortic root with larger AAo, we observed slower backflow towards the sinus and less flow motion within the sinus portion in combination with higher turbulent dissipation in the AAo compared to a normal sized root.

However, we only compared time-averaged flow patterns as well as integral quantities to identify main flow patterns in sinus and AAo. By this, we proposed first hypotheses on sinus washout and platelet activation in larger aortas. This approach was based on averaged Eulerian quantities and did not allow for a quantification of the mechanisms of interest which requires a Lagrangian analysis. Also, the respective role of the neo-sinus must be studied further to assess its impact on sinus washout and platelet activation as it was not considered in our previous study. Therefore, we increase the complexity of our analysis by (a) adding a Lagrangian perspective to the evaluation of sinus washout and platelet activation and (b) comparing the obtained results to a geometrical model that includes a neo-sinus. To also quantify the risk of platelet activation for each particle, we evaluate their individual shear stress history. Our aim is to gain a quantitative understanding of the sinus washout rate and platelet activation levels in an aortic root with and without neo-sinus to better understand the relevance of aortic root morphology in the development of THVT as well as the role of the neo-sinus.

2. Materials and methods

2.1. Parameterized aortic configuration with and without neo-sinus

Two generic aortic models are used to investigate the influence of the aortic root geometry on the flow field. The parameterized aortic model includes three parameters: annular diameter d_A, diameter of the sinotubular junction d_{STJ} and diameter of the ascending aorta d_{AAo} which is measured 40 mm vertically above the aortic annulus (Fig. 1A). The parameters d_{STJ} and d_{AAo} were selected to represent (a) aortic root dimensions found in the general TAVI population unaffected by THVT (control group) and (b) larger aortic root geometries as observed in patients that developed THVT (THVT group). The comparison to a control group establishes causality by isolating the effect of specific parameters (in this case d_{STJ} and d_{AAo}). Table 1 shows the aortic dimensions for each control and THVT model normalized by the annular diameter d_A (22 mm for both groups). Values of the respective parameters were chosen according to results of a previous study [29] which investigated the relevance of aortic root morphology for the development of THVT based on patient data of the Bern TAVI registry (clinicalTrials.gov, identifier: NCT01368250). Details on material models, pressure boundary conditions and valve geometry can be found in [29,30].

Further we assess the role of the neo-sinus which is created by the TAV implantation and describes the region between native leaflets and the prosthetic leaflets. A second fluid–structure interaction simulation is conducted using the previously described THVT aortic model with larger aorta. This control model has been extended by a thin-walled ring which mimics the diseased native leaflets that are pushed outward during TAV implantation (Fig. 1B) such that the neo-sinus is generated between ring and the prosthetic valve leaflets. The ring's thickness is set to 0.75 mm and its height is aligned with the leaflet tips as this configuration presents the worst-case-scenario as it results in the highest volume of stagnation zones as well as the highest remaining number of particles in the sinus after one cycle in comparison to other configurations [31].

2.2. Governing equations and numerical method

The interaction of aortic wall, valve and blood flow is implemented within the high-fidelity solver AV-Flow which is developed for biomedical fluid–structure-interaction (FSI) applications including blood flow and soft tissue on hybrid high-performance computing platforms [32]. The flow field is solved by a fluid solver using a high-order Direct Numerical Simulation (DNS) approach on a grid of $121 \times 257 \times 513$ points. Applying grid stretching to guarantee sufficiently fine spatial resolution at reasonable computational cost, this leads to a minimum mesh width of 150 μm. The time step is set to $\Delta t = 5 \cdot 10^{-6}$s. The fluid is modeled as a Newtonian fluid similar to blood with dynamic viscosity $\mu_f = 0.004$ Pas and density $\rho_f = 1050$ kg/m^3. Field variables such as pressure p_f and velocity $\boldsymbol{u}_f = (u_{f,x}, u_{f,y}, u_{f,z})$ are governed by the incompressible Navier–Stokes equations:

$$\rho_f \frac{\partial \boldsymbol{u}_f}{\partial t} + \rho_f \left(\boldsymbol{u}_f \cdot \nabla\right) \boldsymbol{u}_f + \nabla p_f - \mu_f \Delta \boldsymbol{u}_f = 0 \tag{1}$$

$$\nabla \cdot \boldsymbol{u}_f = 0 \tag{2}$$

The spatial discretization is realized by a 6th-order finite difference scheme while the temporal discretization includes 3rd-order Runge–Kutta time stepping [33].

A finite element solver for soft tissue is applied to the structural part of the FSI problem on an unstructured mesh of approximately 515,000 tetrahedral elements, solving the elastodynamic equations with displacement field $\boldsymbol{u}_s$, density ρ_s and Piola–Kirchhoff stress tensor $\boldsymbol{P}$

$$\rho_s \frac{\partial^2 \boldsymbol{u}_s}{\partial t^2} - \nabla \cdot \boldsymbol{P} = 0 \tag{3}$$

An implicit, partitioned coupling scheme with a modified Immersed-Boundary method based on variational transfer realizes the coupling of fluid and structure motion. Interface conditions are described by

$$\boldsymbol{u}_f = \frac{\partial \boldsymbol{u}_s}{\partial t} \tag{4}$$

$$\boldsymbol{J}^{-1} \boldsymbol{P} \boldsymbol{F}^T \boldsymbol{n} = \boldsymbol{\sigma}_f \boldsymbol{n} \tag{5}$$

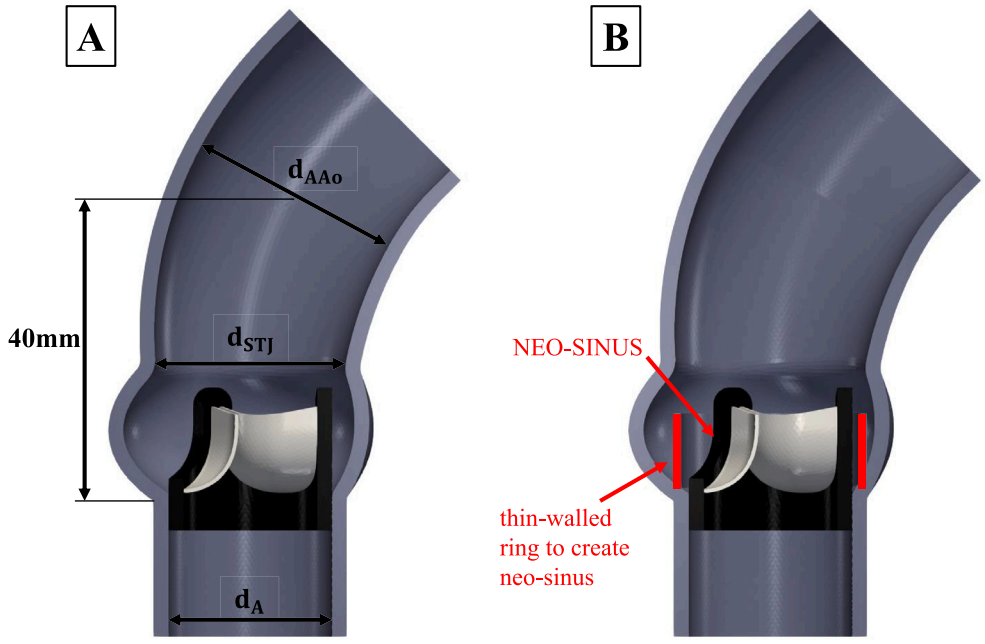

Fig. 1. (A) Schematic representation of the parameterized generic aortic geometry with biological tissue valve and variable parameters: diameter of the sinotubular junction (d_{STJ}) and diameter of the ascending aorta (d_{AAo}) relative to the constant annular diameter ($d_A = 22$ mm). Edited from [29]. (B) Parameterized aortic geometry featuring a thin-walled ring aligned with the leaflet height to model the neo-sinus.

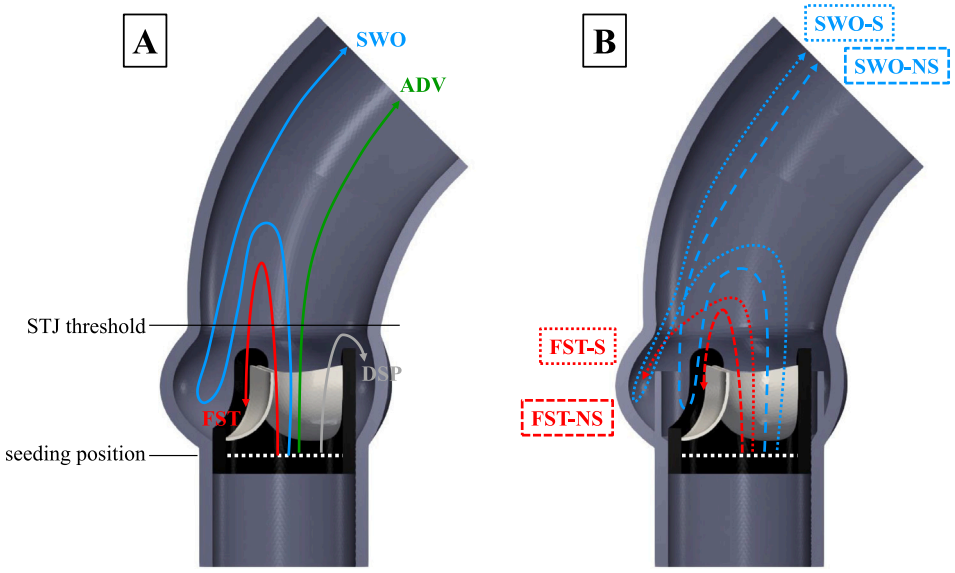

Fig. 2. (**A**): Schematic representation of particle categorization according to their time-dependent trajectory with seeding position and STJ threshold located at $z = 0.01$ m. Particles are categorized into groups: advection (ADV, green), sinus washout (SWO, blue), flow stagnation (FST, red) and directly sinus portion (DSP, gray). (**B**): Additional particle categorization for configuration with neo-sinus. Sinus washout (SWO) and flow stagnation (FST) groups are divided based if they enter the neo-sinus (SWO-NS, dashed blue/FST-NS, dashed red) or the native sinus (SWO-S, dotted blue/FST-S, dotted red).

with $\boldsymbol{F} = \nabla \boldsymbol{u}_s + \boldsymbol{I}$, its associated determinant $J = \det \boldsymbol{F}$ and the Cauchy stress of the fluid $\boldsymbol{\sigma}_f$. For details on the high-fidelity FSI solver and its experimental and numerical validation, see [30,32].

2.3. Lagrangian particle tracing and assessment of platelet activation

Lagrangian particle tracing is performed to quantify the washout of the sinus portions as well as flow stagnation. A total of 959 mass-less particles are initially distributed equidistantly in a cross-section normal to the inflow issuing from the left ventricular outflow tract (LVOT) immediately upstream of the valve. This initial distribution of particles is released periodically at time increments of $\Delta t = 0.005$ s starting from a time instance of $t_0 = 0.1$ s and traced for a time period of $T = 0.2$ s until $t_1 = 0.3$ s.

Particles are then categorized into four groups depending on their time-dependent trajectories relative to the sinotubular junction (STJ) threshold at $z = 0.01$ m (Fig. 2A):

- **ADV**ection (ADV): Purely advected particles that are directly leaving the fluid domain through the AAo
- **S**inus**W**ash**O**ut (SWO): Particles contributing to the sinus washout by first entering the AAo with the aortic jet, then flowing back to the sinus along the aortic wall and finally exiting the sinus towards the AAo

- **F**low**ST**agnation (FST): Particles entering the AAo with the aortic jet, flowing back to the sinus and stagnating there
- **D**irectly**S**inus**P**ortions (DSP): Particles immediately entering and remaining in the sinus without crossing the STJ threshold

We consider the FST category as the most risky group in terms of thrombus formation. In this category, particles enter the turbulent aortic jet and pass through a region of elevated shear stresses in the AAo. Then, they enter the retrograde flow region along the aortic wall, flowing back to the sinus where they eventually stagnate. This combines two main hemodynamic factors leading to thrombosis: platelet activation by high shear stresses and successive stagnation.

For the configuration with neo-sinus in Fig. 2B, the categories for sinus washout (SWO) and flow stagnation (FST) were further divided depending on whether they enter the neo-sinus (SWO-NS/FST-NS) or native sinus (SWO-S/FST-S). Particles directly entering the neo-sinus or native sinus, respectively, are cumulated in one DSP category as they are considered less relevant for platelet activation since they never enter the high-shear stress regions in the AAo.

To assess the risk of thrombus formation originating from the various particle categories, we compute a respective indicator for platelet activation for the traced particles. A model calculating blood damage indices (BDI) accounting for the cumulative shear stresses on red blood cells during unsteady flow behavior is implemented according to [34] in its discrete form

$$BDI = \sum_{i=1}^{N} Ca \left[\sum_{j=1}^{i} \tau\left(t_j\right)^{b/a} \Delta t_j + D\left(t_0\right) \right]^{a-1} \tau\left(t_i\right)^{b/a} \Delta t_i \tag{6}$$

for N observation time intervals. The term $\tau\left(t_i\right)^{b/a} \Delta t_i$ describes the incremental mechanical dose experienced from time instant t_{i-1} to t_i which is considered constant. The term in brackets accounts for the shear-stress history of each red blood cell by calculating the accumulated mechanical dose from the initial observation time instant until t_i [34] with the initial dose $D\left(t_0\right)$ which is neglected here. The model was modified according to [19] to evaluate the platelet activation index $\mathrm{BDI}_{\mathrm{platelet}}$ by setting the non-dimensional constants to $a = 1.3198, b = 0.6256$ and $C = 1.0 \cdot 10^{-5}$.

Statistical differences between the different particle categories were tested with the Wilcoxon rank-sum test and p-values below 0.05 were considered significant.

3. Results

3.1. General flow patterns and viscous shear stress distributions

During systolic acceleration, the valve opens and the aortic jet emerges from the valve orifice. The aortic jet impinges on the outer aortic wall due to AAo curvature resulting in retrograde flow along the aortic wall towards the sinus portions (Fig. 3A).

Animated particle pathways initiated immediately above the valve orifice can be found in the supplementary material which contribute to a three-dimensional understanding of existing flow patterns. Besides the forward aortic jet which deflects at the AAo curvature, we can observe the retrograde flow along the aortic wall which exists even in a considerable downstream distance of the valve. Also, the animation shows that the sinus washout is limited to a region close to the valve leaflets while particles tend to stagnate in the outer part of the sinus portions. Last, we can appreciate the helical flow in the AAo due to Dean vortices formed at the outer curvature of the beginning of the aortic arch.

The velocity gradient between forward flow of the aortic jet and backward flow along the aortic wall results in a shear layer between those two regions exhibiting turbulent fluctuations. Fig. 3B displays the time-averaged viscous shear stresses during peak systole for control model without neo-sinus, THVT model without neo-sinus and THVT model with neo-sinus. All configurations show similar qualitative averaged shear stress patterns in the AAo that are typical for turbulent jet flow.

Fig. 3C shows histograms of the instantaneous shear stresses at $t = 0.3$ s to quantify the range of viscous shear stresses a particle could experience instantaneously. The comparison of control and THVT model without neo-sinus reveals similar distributions with a higher amount of low shear stresses in the THVT case. At higher shear stress values, we observe a slightly higher amount for the control group. The neo-sinus, however, does not significantly influence the instantaneous viscous shear stress distribution in the AAo.

Yet, not only elevated shear stresses at one time instant can lead to platelet activation, but also the accumulation of moderate shear stresses over a longer time period. This scenario cannot be evaluated by Eulerian quantities alone, but needs to be assessed by a Lagrangian approach tracking each individual particle over time.

Table 2
Percentages of particles for control and THVT model without neo-sinus and THVT model with neo-sinus for categories advection (ADV), sinus washout (SWO), flow stagnation (FST) and directly sinus portion (DSP). For the case with neo-sinus, SWO and FST are sub-categorized based on entering the neo-sinus (SWO-NS/FST-NS) or the native sinus (SWO-S/FST-S). The "relative stagnation ratio" $\left(\frac{\mathrm{FST+DSP}}{\mathrm{SWO+FST+DSP}}\right)$ indicates which relative percentage of particles flowing back to the sinus portions ("backflow to sinus", SWO+FST+DSP) eventually stagnates there.

	Without neo-sinus		With neo-sinus
	Control	THVT	THVT
Advection (ADV)	82.3	86.7	86.1
Sinus washout (SWO)	7.4	4.9	NS: 2.2 S: 2.6
Flow stagnation (FST)	6.2	4.4	NS: 2.1 S: 5.2
Directly sinus portion (DSP)	4.2	3.9	1.8
Backflow to sinus (SWO+FST+DSP)	17.7	13.1	NS: 4.9 S: 9.0
relative stagnation ratio $\left(\frac{\mathrm{FST+DSP}}{\mathrm{SWO+FST+DSP}}\right)$	58.4	62.9	NS: 55.0 S: 71.3

3.2. Lagrangian particle tracing and washout quantification

Table 2 shows the particle percentages per category for the THVT configuration and the control. Most particles are directly advected downstream (ADV) through the ascending aorta after passing the valve orifice without passing the STJ threshold again in the observation time period. However, more particles are directly advected in the THVT model compared to the control model (+5.3%). The neo-sinus (NS) does not seem to influence the number of advected particles (without NS: 86.7%, with NS: 86.1%). Particles entering the sinus portions directly (DSP) are similar for both models without neo-sinus (3.9% for THVT without NS vs. 4.2% for control without NS) and even lower in case of a neo-sinus (1.8% for THVT with NS).

The amount of particles contributing to sinus washout (SWO) are considerably lower for both THVT configurations (−34.1% without NS and −34.9% with NS compared to control). For the THVT model with neo-sinus, the washout is nearly equally divided between neo-sinus and native sinus (NS: 2.2% vs. S: 2.6%).

The highest amount of particles experiencing high shear stresses in the AAo and then stagnating in the sinus (FST) can be found in the THVT configuration with neo-sinus (in total 7.3%) with more particles stagnating in the native sinus (NS: 2.1% vs. S: 5.2%). The control group without neo-sinus shows the second largest amount (6.2%) followed by the THVT group without neo-sinus (4.4%).

The total amount of particles flowing back along the aortic wall to the sinus is highest for the control group (17.7%) and lower for THVT without neo-sinus (13.1%) and with neo-sinus (13.9%). However, particles that have entered the native sinus have a higher likelihood of stagnating there for the THVT configurations (THVT without NS: +7.7%, THVT with NS: +22.0%) than for the control.

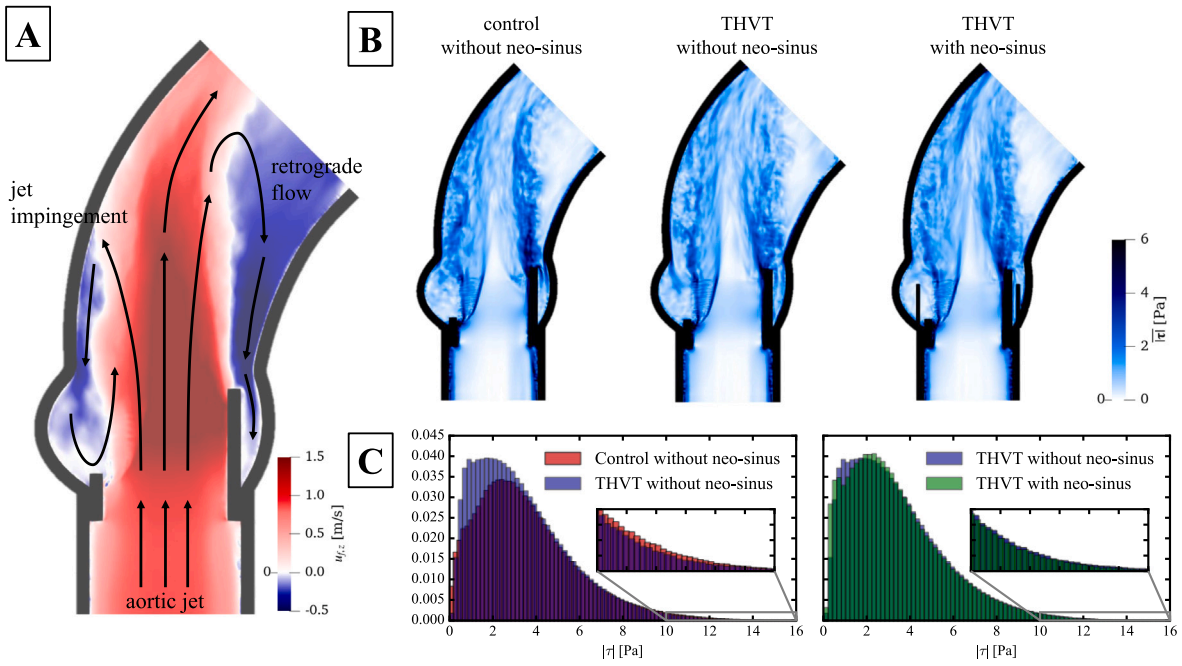

Fig. 3. (A) Schematic illustration on general flow trajectories with the aortic jet issuing from the LVOT visualized by the time-averaged streamwise velocity field. After passing through the valve, the aortic jet impinges at the aortic wall resulting in retrograde flow towards the sinus. The AAo curvature leads to a deflection of the aortic jet. (B) Time-averaged viscous shear stresses at peak systole for control and THVT model without neo-sinus as well as THVT model with neo-sinus. (C) Histograms of instantaneous viscous shear stresses within the AAo at $t = 0.3$ s for (left) control and THVT model without neo-sinus and (right) THVT model with and without neo-sinus.

3.3. Evaluation of platelet activation potential

Fig. 4 shows the distribution of the accumulated platelet activation index $BDI_{platelet}$ at the final position of each particle for control (control), THVT model without (THVT w/oNS) and with neo-sinus (THVT wNS) categorized in the previously defined particle groups.

Purely advective particles (ADV) show the same trend for both control and THVT model without neo-sinus with rather low $BDI_{platelet}$ and many outliers towards higher values. Medians are similar with $0.29 \cdot 10^{-6}$ (IQR: $[0.15, 0.59] \cdot 10^{-6}$) for control and $0.27 \cdot 10^{-6}$ (IQR: $[0.14, 0.55] \cdot 10^{-6}$) for THVT. The similar relative amount of advective particles in the THVT model with neo-sinus generally has higher $BDI_{platelet}$ with a median of $0.77 \cdot 10^{-6}$ (IQR: $[0.43, 1.47] \cdot 10^{-6}$).

Particles stagnating directly in the sinus (DSP) show low accumulated $BDI_{platelet}$ in general as they do not enter the region of the ascending aorta which presents the highest shear stress values and therefore the highest activation potential. Also here, medians for control and THVT group are comparable with $0.25 \cdot 10^{-6}$ (IQR: $[0.14, 0.52] \cdot 10^{-6}$) and $0.32 \cdot 10^{-6}$ (IQR: $[0.19, 0.57] \cdot 10^{-6}$), respectively, with many outliers at higher values. The THVT configuration with neo-sinus shows a higher median with $1.31 \cdot 10^{-6}$ (IQR: $[0.98, 1.63] \cdot 10^{-6}$) which can be related to numerical artifacts.

Differences between the $BDI_{platelet}$ of particles contributing to sinus washout (SWO) are not statistically significant ($p > 0.05$) when comparing the control model (median: $1.44 \cdot 10^{-6}$, IQR: $[1.08, 1.95] \cdot 10^{-6}$) to the THVT model without neo-sinus ($1.53 \cdot 10^{-6}$, IQR: $[1.06, 1.98] \cdot 10^{-6}$). Particles contributing to the sinus washout in the THVT case with neo-sinus are divided into washout of the neo-sinus (SWO-NS) and washout of the native sinus (SWO-S). Both value ranges are similar (SWO-NS: median $2.10 \cdot 10^{-6}$ with IQR $[1.84, 2.32] \cdot 10^{-6}$, SWO-S: median $2.08 \cdot 10^{-6}$ with IQR $[1.78, 2.27] \cdot 10^{-6}$), however, values are in general significantly higher than the configurations without neo-sinus ($p < 0.05$).

Statistically significant differences ($p < 0.05$) are observed for the flow stagnation (FST) group. FST particles might present the highest risk in the context of thrombus formation as these particles experienced high stresses in the ascending aorta and then stagnate in the sinus. Comparing configurations without neo-sinus, the THVT group shows a smaller data range of $BDI_{platelet}$ values ($2.39 \cdot 10^{-6}$ vs. $2.77 \cdot 10^{-6}$ for control), however, the median ($1.48 \cdot 10^{-6}$ for THVT vs. $1.06 \cdot 10^{-6}$ for control) is significantly larger ($p < 0.05$) and the interquartile range is shifted towards higher values compared to the control group ($[0.97, 1.88] \cdot 10^{-6}$ for THVT vs. $[0.46, 1.75] \cdot 10^{-6}$ for control). For the THVT model with neo-sinus, particles stagnating in the native sinus show similar $BDI_{platelet}$ values (median $1.54 \cdot 10^{-6}$, IQR $[1.24, 1.83] \cdot 10^{-6}$) compared to the THVT group without neo-sinus. However, particles stagnating in the neo-sinus present a significantly higher median of $1.91 \cdot 10^{-6}$ and an interquartile range shifted to higher values (IQR: $[1.72, 2.21] \cdot 10^{-6}$).

4. Discussion

In this computational study, we conducted Lagrangian particle tracing and assessed platelet activation to test first hypotheses on the relation between aortic morphology and THVT based on mean flow features as reported in our previous study [29]. Fluid–structure interaction simulations of two generic aortic root models with an inserted tissue valve were performed: A larger aortic model representing THVT patients (THVT model) and a smaller aortic model representing unaffected TAVI patients (control model). Additionally, we conducted simulations for the larger aortic root geometry including a neo-sinus. To quantify the washout of the sinus portion, Lagrangian particle tracing and classification of particles according to their pathway during peak systole was performed. The accumulation of shear stresses by each particle was assessed to formulate distributions of platelet activation indices per category and better quantify the risk of platelet activation and eventually thrombus formation.

As visible in the animated particle pathways in the supplementary material, an aortic jet emerges from the valve orifice and impinges at the aortic wall creating backflow to the sinus. A shear layer is created between the forward aortic jet and the retrograde flow, resulting in elevated shear stresses in the ascending aorta. These elevated shear stresses have been reported for multiple valve prostheses by Yoganathan et al. [35]. Hedayat et al. [36] suggested the significant role of the bulk flow issuing from the aortic valve in the risk of platelet

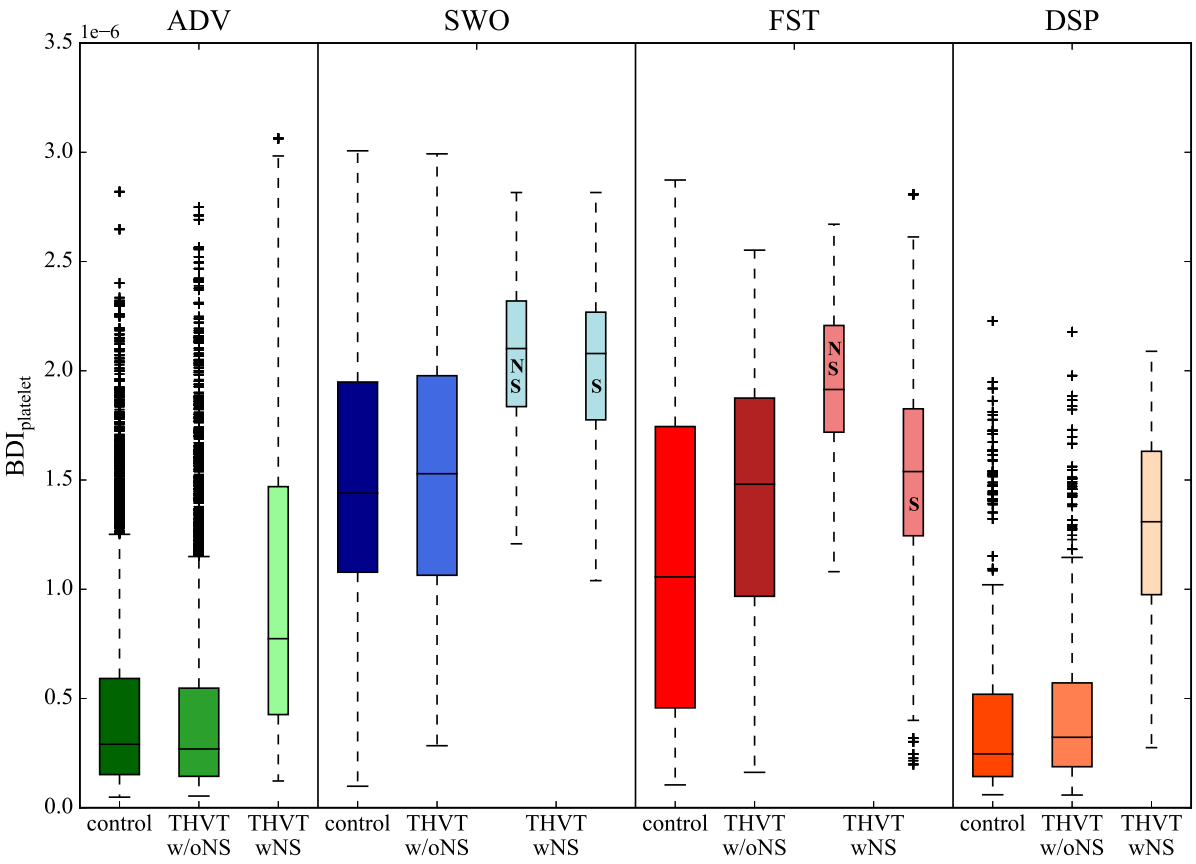

Fig. 4. Distribution of the accumulated particle activation index $BDI_{platelet}$ at the final position for the time period 0.1 s to 0.3 s divided in particle categories advection (ADV, green), sinus washout (SWO, blue), flow stagnation (FST, red) and directly sinus portion (DSP, orange). Results are shown for control model without neo-sinus (control), THVT model without (THVT w/oNS) and with neo-sinus (THVT wNS). Categories for THVT wNS are further divided into washout of the neo-sinus (SWO-NS) and the native sinus (SWO-S) as well as flow stagnation in the neo-sinus (FST-NS) and the native sinus (FST-S).

activation during the systolic phase. During peak systole, flow motion in the sinus cavities was shown to depend on the intensity of the aortic jet and the sinus geometry [21]. As already discussed in our previous study [29], a larger AAo allows for a widening of the aortic jet which also results in larger regions of elevated shear stresses (Fig. 3B). However, this only leads to larger regions of moderately elevated shear stress values while regions of potentially critical stress values remain of comparable size independently of the AAo geometry or the neo-sinus (Fig. 3C).

By Lagrangian tracing of mass-less particles (see also the supplementary video), we could follow and categorize their individual pathways and evaluate how many particles are advected, contribute to the sinus washout or stagnate in the sinus. Results reveal that the more particles contribute to the washout in the control model compared to a larger aorta which leads to a lower washout rate for the THVT model (−34.1%). For the THVT model with neo-sinus, the reduced washout rate (−34.9% less than in control) is equally split between sinus and neo-sinus.

Although the risk of stagnation after entering the sinus is highest in the native sinus of both THVT models, absolute values are highest in the control model and the least in the neo-sinus of the THVT model. This raises the question whether the total amount is relevant in assessing the risk for thrombosis or whether the activation levels of the stagnating particles are more relevant. Indeed, the smallest amount of stagnating particles in the neo-sinus of the THVT model was found to have significantly higher activation levels compared to any other group with +29.1% for THVT without neo-sinus, +24.0% in the native sinus of THVT with neo-sinus and even +80.2% for the control. Although fewer particles are stagnating in the sinus of the THVT models, the larger aorta seems to lead to higher activation levels of stagnating particles than for the normal aorta. Our findings of a larger aorta increasing the risk for thrombosis are consistent with a recent study by Oks et al. [27]. Here, the model with the largest STJ diameter leads to the highest residence time of flow in the sinus portion as well as increased platelet stress accumulation compared to smaller STJ diameters. The observation of higher risk of potential thrombus formation in a configuration with neo-sinus (TAV) compared to one without (surgical aortic valve) is in line with clinical reports stating a higher likelihood of leaflet thrombosis in TAV patients (up to 35% [2,6–9]) than patients with surgical valve prostheses (up to 4.0% [37,38]). Significantly higher platelet activation levels for particles stagnating in the neo-sinus could also provide an explanation for the occurrence of thrombi particularly in the neo-sinus region [5,8,39].

In [29], we proposed first hypotheses on the relation between thrombus formation and a larger aortic root based on mean flow patterns. Lower backflow velocities, higher backflow rate and less motion in the sinus were suggesting a lower sinus washout rate. In combination with higher turbulent dissipation rate in the AAo, we postulated that the combination of platelet activation in the AAo and flow stagnation in the sinus promotes thrombosis formation in larger aortas. In this current study, we confirmed these hypotheses by quantitative Lagrangian data showing less efficient sinus washout and higher platelet activation levels for stagnating particles in larger aortas of THVT patients.

Limitations

The computational study is limited by the idealized generic aortic root configuration excluding large variations in individual patient morphology. However, by choosing the parameterization values of the ascending aorta according to our previously conducted pilot study

based on patient data [29], we ensure the physiological plausibility of the applied geometries. Moreover, parameterized generic configurations allow the systematic study of particular aortic root features on the flow field as in this case, aortic diameters.

In this study, only systolic acceleration towards peak systole was simulated. We consider this phase of the cardiac cycle most relevant when assessing platelet activation, because highest values of viscous shear stresses and highest intensity of turbulent fluctuations are observed in the AAo during peak systole. Nevertheless, it may be helpful to extend the present study also to the diastolic phase which may show additional particle stagnation.

The lack of coronary flow and coronaries in the performed FSI study is expected to change the flow in the sinus portions. However, several studies found less flow along the sinus base and a higher proneness to stagnation for the non-coronary cusp [40,41]. Therefore, results of this study might underestimate the actual sinus washout in an aortic root with coronaries.

5. Conclusions

The occurrence of high shear stresses in the ascending aorta was comparable between both normal (control) and larger aorta (THVT) as well as configurations with and without neo-sinus. However, Lagrangian particle tracing revealed a lower washout efficiency in the larger aortic root of THVT patients. Although fewer particles stagnated in the sinus of the THVT model, platelet activation indices were significantly higher for stagnating particles in the native sinus and especially high for particles stagnating in the neo-sinus of the larger aortic root. These observations could provide an explanation for (a) a higher occurrence of thrombus formation in transcatheter valves compared to surgical valves without neo-sinus and (b) the aortic side of the leaflet in the neo-sinus as the prevalent region for thrombi.

During the pre-procedural CT scan, aortic diameters are measured routinely to plan the intervention. With the knowledge gained from our findings, these measurements could help to identify patients at higher thrombosis risk before the actual procedure. After surgery, the awareness of possibly higher thrombosis risk facilitates the choice of a suitable anti-coagulation scheme. However, a wider range of aortic diameters should be evaluated to extend our understanding of blood flow patterns which is presently limited to two specific geometrical parameter sets representing patients with and without THVT. This way, a specific threshold above which a patient may be subjected to increased thrombosis risk can be identified, improving clinical guidelines and supporting clinicians in their pre- and post-surgical decision-making.

CRediT authorship contribution statement

Karoline-Marie Bornemann: Writing – review & editing, Writing – original draft, Visualization, Software, Methodology, Formal analysis, Data curation, Conceptualization. **Silje Ekroll Jahren:** Writing – review & editing, Methodology, Conceptualization. **Dominik Obrist:** Writing – review & editing, Supervision, Methodology, Funding acquisition, Conceptualization.

Declaration of competing interest

None declared.

Data availability

The data that support the findings of this study are available from the corresponding author upon reasonable request.

Acknowledgments

The authors acknowledge Guillaume Van Rossem who contributed to this work by developing post-processing tools for data analysis.

Funding

This work was supported by a grant from the Swiss National Supercomputing Centre (CSCS), Switzerland under project ID s1186.

Appendix A. Supplementary data

Supplementary material related to this article can be found online at https://doi.org/10.1016/j.compbiomed.2024.108828.

References

[1] A. Kataruka, C.M. Otto, Valve durability after transcatheter aortic valve implantation, J. Thoracic Dis. 10 (2018) S3629–S3636, http://dx.doi.org/10.21037/jtd.2018.07.38.

[2] L. Rosseel, O. De Backer, L. Søndergaard, Clinical valve thrombosis and subclinical leaflet thrombosis following transcatheter aortic valve replacement: Is there a need for a patient-tailored antithrombotic therapy? Front. Cardiovasc. Med. 6 (2019) 1–10, http://dx.doi.org/10.3389/fcvm.2019.00044, URL https://www.frontiersin.org/article/10.3389/fcvm.2019.00044/full.

[3] A. Franzone, T. Pilgrim, A.G. Haynes, J. Lanz, M. Asami, F. Praz, L. Raber, E. Roost, B. Langhammer, S. Windecker, S. Stortecky, L. Räber, E. Roost, B. Langhammer, S. Windecker, S. Stortecky, Transcatheter aortic valve thrombosis: Incidence, clinical presentation and long-term outcomes, Eur. Heart J. Cardiovascular Imaging 19 (2018) 398–404, http://dx.doi.org/10.1093/ehjci/jex181, URL https://academic.oup.com/ehjcimaging/article/19/4/398/4056170.

[4] J. Jose, D.S. Sulimov, M. El-Mawardy, T. Sato, A. Allali, E.W. Holy, B. Becker, M. Landt, J. Kebernik, B. Schwarz, G. Richardt, M. Abdel-Wahab, Clinical bioprosthetic heart valve thrombosis after transcatheter aortic valve replacement incidence, characteristics, and treatment outcomes, JACC: Cardiovasc. Intervent. 10 (2017) 686–697.

[5] A. Latib, T. Naganuma, M. Abdel-Wahab, H. Danenberg, L. Cota, M. Barbanti, H. Baumgartner, A. Finkelstein, V. LeGrand, J.S.D. Lezo, J. Kefer, D. Messika-Zeitoun, G. Richardt, E. Stabile, G. Kaleschke, A. Vahanian, J.C. Laborde, M.B. Leon, J.G. Webb, V.F. Panoulas, F. Maisano, O. Alfieri, A. Colombo, Treatment and clinical outcomes of transcatheter heart valve thrombosis, Circulation: Cardiovasc. Intervent. 8 (2015) e001779, http://dx.doi.org/10.1161/CIRCINTERVENTIONS.114.001779.

[6] S. Garcia, M. Fukui, M.W. Dworak, B.K. Okeson, R. Garberich, G. Hashimoto, H. Sato, J.L. Cavalcante, V.N. Bapat, J. Lesser, V. Cheng, M.C. Newell, M. Goessl, S. Elmariah, S.M. Bradley, P. Sorajja, Clinical impact of hypoattenuating leaflet thickening after transcatheter aortic valve replacement, Circulation: Cardiovascular Intervent. 15 (2022) 303–312, http://dx.doi.org/10.1161/CIRCINTERVENTIONS.121.011480.

[7] N.C. Hansson, E.L. Grove, H.R. Andersen, J. Leipsic, O.N. Mathiassen, J.M. Jensen, K.T. Jensen, P. Blanke, T. Leetmaa, M. Tang, L.R. Krusell, K.E. Klaaborg, E.H. Christiansen, K. Terp, C.J. Terkelsen, S.H. Poulsen, J. Webb, H.E. Bøtker, B.L. Nørgaard, Transcatheter aortic valve thrombosis, J. Am. College Cardiol. 68 (2016) 2059–2069, http://dx.doi.org/10.1016/j.jacc.2016.08.010.

[8] R.R. Makkar, G. Fontana, H. Jilaihawi, T. Chakravarty, K.F. Kofoed, O.D. Backer, F.M. Asch, C.E. Ruiz, N.T. Olsen, A. Trento, J. Friedman, D. Berman, W. Cheng, M. Kashif, V. Jelnin, C.A. Kliger, H. Guo, A.D. Pichard, N.J. Weissman, S. Kapadia, E. Manasse, D.L. Bhatt, M.B. Leon, L. Søndergaard, Possible subclinical leaflet thrombosis in bioprosthetic aortic valves, New England J. Med. 373 (2015) 2015–2024, http://dx.doi.org/10.1056/NEJMoa1509233.

[9] R. Yanagisawa, K. Hayashida, Y. Yamada, M. Tanaka, F. Yashima, T. Inohara, T. Arai, T. Kawakami, Y. Maekawa, H. Tsuruta, Y. Itabashi, M. Murata, M. Sano, K. Okamoto, A. Yoshitake, H. Shimizu, M. Jinzaki, K. Fukuda, Incidence, predictors, and mid-term outcomes of possible leaflet thrombosis after TAVR, JACC: Cardiovasc. Imag. 10 (2017) 1–11, http://dx.doi.org/10.1016/j.jcmg.2016.11.005.

[10] V. Raghav, P. Midha, R. Sharma, V. Babaliaros, A. Yoganathan, Transcatheter aortic valve thrombosis: a review of potential mechanisms, J. R. Soc. Interface 18 (2021) http://dx.doi.org/10.1098/rsif.2021.0599.

[11] F. Khodaee, M. Barakat, M. Abbasi, D. Dvir, A.N. Azadani, Incomplete expansion of transcatheter aortic valves is associated with propensity for valve thrombosis, Interact. Cardiovasc. Thoracic Surgery 30 (2020) 39–46, http://dx.doi.org/10.1093/icvts/ivz213.

[12] L. Pietrasanta, S. Zheng, D.D. Marinis, D. Hasler, D. Obrist, Characterization of turbulent flow behind a transcatheter aortic valve in different implantation positions, Front. Cardiovasc. Med. 8 (2022) 1–15, http://dx.doi.org/10.3389/fcvm.2021.804565.

[13] D. Pott, A. Sedaghat, C. Schmitz, N. Werner, T. Schmitz-Rode, U. Steinseifer, S.V. Jansen, Hemodynamics inside the neo- and native sinus after TAVR: Effects of implant depth and cardiac output on flow field and coronary flow, Artif. Organs. 45 (2021) 68–78, http://dx.doi.org/10.1111/aor.13789.

[14] P.M. Trusty, S.S. Bhat, V. Sadri, M.T. Salim, E. Funnell, N. Kamioka, R. Sharma, R. Makkar, V. Babaliaros, A.P. Yoganathan, The role of flow stasis in transcatheter aortic valve leaflet thrombosis, J. Thorac. Cardiovasc. Surg. 164 (2022) e105–e117, http://dx.doi.org/10.1016/J.JTCVS.2020.10.139.

[15] Y. Ahmad, R. Makkar, L. Sondergaard, Hypoattenuated leaflet thickening (HALT) and reduced leaflet motion (RELM) of aortic bioprostheses: An imaging finding or a complication? Progr. Cardiovascular Dis. 72 (2022) 78–83, http://dx.doi.org/10.1016/j.pcad.2022.05.007.

[16] P. Blanke, J.A. Leipsic, J.J. Popma, S.J. Yakubov, G.M. Deeb, H. Gada, M. Mumtaz, B. Ramlawi, N.S. Kleiman, P. Sorajja, J. Askew, C.U. Meduri, J. Kauten, S. Melnitchouk, I. Inglessis, J. Huang, M. Boulware, M.J. Reardon, Bioprosthetic aortic valve leaflet thickening in the evolut low risk sub-study, J. Am. College Cardiol. 75 (2020) 2430–2442, http://dx.doi.org/10.1016/j.jacc.2020.03.022.

[17] M. Hein, S. Schoechlin, U. Schulz, J. Minners, P. Breitbart, C. Lehane, F.-J. Neumann, P. Ruile, Long-term follow-up of hypoattenuated leaflet thickening after transcatheter aortic valve replacement, JACC: Cardiovasc. Intervent. 15 (2022) 1113–1122, http://dx.doi.org/10.1016/j.jcin.2022.04.018.

[18] J. Nicolas, G. Dangas, Hypoattenuated leaflet thickening after transcatheter aortic valve replacement: Additional data, yet still many unanswered questions, Circulat. Cardiovasc. Intervent. 15 (2022) 313–316, http://dx.doi.org/10.1161/CIRCINTERVENTIONS.122.011828.

[19] M. Nobili, J. Sheriff, U. Morbiducci, A. Redaelli, D. Bluestein, Platelet activation due to hemodynamic shear stresses: Damage accumulation model and comparison to in vitro measurements, ASAIO J. 54 (2008) 64–72, http://dx.doi.org/10.1097/MAT.0b013e31815d6898.

[20] S.C. Shadden, S. Hendabadi, Potential fluid mechanic pathways of platelet activation, Biomech. Model. Mechanobiol. 12 (2013) 467–474, http://dx.doi.org/10.1007/s10237-012-0417-4.

[21] H. Hatoum, S. Singh-Gryzbon, F. Esmailie, P. Ruile, F.J. Neumann, P. Blanke, V.H. Thourani, A.P. Yoganathan, L.P. Dasi, Predictive model for thrombus formation after transcatheter valve replacement, Cardiovasc. Eng. Technol. 12 (2021) 576–588, http://dx.doi.org/10.1007/s13239-021-00596-x.

[22] H. Hatoum, J. Dollery, S.M. Lilly, J. Crestanello, L.P. Dasi, Impact of patient-specific morphologies on sinus flow stasis in transcatheter aortic valve replacement: An in vitro study, J. Thoracic Cardiovascular Surgery 157 (2019) 540–549, http://dx.doi.org/10.1016/j.jtcvs.2018.05.086.

[23] I.D. Madukauwa-David, V. Sadri, P.A. Midha, V. Babaliaros, C. Aidun, A.P. Yoganathan, An evaluation of the influence of coronary flow on transcatheter heart valve neo-sinus flow stasis, Ann. Biomed. Eng. 48 (2020) 169–180, http://dx.doi.org/10.1007/s10439-019-02324-y.

[24] S. Singh-Gryzbon, B. Ncho, V. Sadri, S.S. Bhat, S.S. Kollapaneni, D. Balakumar, Z.A. Wei, P. Ruile, F.-J.J. Neumann, P. Blanke, A.P. Yoganathan, Influence of patient-specific characteristics on transcatheter heart valve neo-sinus flow: An in silico study, Ann. Biomed. Eng. 48 (2020) 2400–2411, http://dx.doi.org/10.1007/s10439-020-02532-x.

[25] D. Hasler, D. Obrist, Three-dimensional flow structures past a bioprosthetic valve in an in-vitro model of the aortic root, PLoS ONE 13 (2018) e0194384, http://dx.doi.org/10.1371/journal.pone.0194384.

[26] S.E. Jahren, P.P. Heinisch, D. Hasler, B.M. Winkler, S. Stortecky, T. Pilgrim, M.C. Londono, T. Carrel, H.V. Tengg-Kobligk, D. Obrist, Can bioprosthetic valve thrombosis be promoted by aortic root morphology? An in vitro study, Interact. Cardiovasc. Thoracic Surgery 27 (2018) 108–115, http://dx.doi.org/10.1093/icvts/ivy039.

[27] D. Oks, S. Reza, M. Vázquez, G. Houzeaux, B. Kovarovic, C. Samaniego, D. Bluestein, Effect of sinotubular junction size on TAVR leaflet thrombosis: A fluid-structure interaction analysis, Ann. Biomed. Eng. 52 (2024) 719–733.

[28] D. Tomii, T. Okuno, D. Heg, C. Gräni, J. Lanz, F. Praz, S. Stortecky, S. Windecker, T. Pilgrim, D. Reineke, Sinus of valsalva dimension and clinical outcomes in patients undergoing transcatheter aortic valve implantation, Am. Heart J. 244 (2022) 94–106, http://dx.doi.org/10.1016/j.ahj.2021.11.004, URL https://linkinghub.elsevier.com/retrieve/pii/S0002870321004476.

[29] S. Jahren, C. Demirel, K.-M. Bornemann, P. Corso, S. Stortecky, D. Obrist, Altered blood flow due to larger aortic diameters in patients with transcatheter heart valve thrombosis, APL Bioeng. 7 (2023) 046120.

[30] B. Becsek, L. Pietrasanta, D. Obrist, Turbulent systolic flow downstream of a bioprosthetic aortic valve: Velocity spectra, wall shear stresses, and turbulent dissipation rates, Front. Physiol. 11 (2020) 1–19, http://dx.doi.org/10.3389/fphys.2020.577188.

[31] P.A. Midha, V. Raghav, R. Sharma, J.F. Condado, I.U. Okafor, T. Rami, G. Kumar, V.H. Thourani, H. Jilaihawi, V. Babaliaros, R.R. Makkar, A.P. Yoganathan, The fluid mechanics of transcatheter heart valve leaflet thrombosis in the neosinus, Circulation 136 (2017) 1598–1609, http://dx.doi.org/10.1161/CIRCULATIONAHA.117.029479.

[32] M.G.C. Nestola, B. Becsek, H. Zolfaghari, P. Zulian, D.D. Marinis, R. Krause, D. Obrist, An immersed boundary method for fluid-structure interaction based on variational transfer, J. Comput. Phys. 398 (2019) 108884, http://dx.doi.org/10.1016/j.jcp.2019.108884.

[33] R. Henniger, D. Obrist, L. Kleiser, High-order accurate solution of the incompressible Navier-Stokes equations on massively parallel computers, J. Comput. Phys. 229 (2010) 3543–3572, http://dx.doi.org/10.1016/j.jcp.2010.01.015.

[34] M. Grigioni, U. Morbiducci, G. D'Avenio, G. Di Benedetto, C.D. Gaudio, A novel formulation for blood trauma prediction by a modified power-law mathematical model, Biomech. Model. Mechanobiol. 4 (2005) 249–260, http://dx.doi.org/10.1007/s10237-005-0005-y.

[35] A.P. Yoganathan, Z. He, S.C. Jones, Fluid mechanics of heart valves, Annu. Rev. Biomed. Eng. 6 (2004) 331–362, http://dx.doi.org/10.1146/annurev.bioeng.6.040803.140111.

[36] M. Hedayat, H. Asgharzadeh, I. Borazjani, Platelet activation of mechanical versus bioprosthetic heart valves during systole, J. Biomech. 56 (2017) 111–116, http://dx.doi.org/10.1016/j.jbiomech.2017.03.002, https://linkinghub.elsevier.com/retrieve/pii/S0021929017301355.

[37] T. Chakravarty, L. Søndergaard, J. Friedman, O.D. Backer, D. Berman, K.F. Kofoed, H. Jilaihawi, T. Shiota, Y. Abramowitz, T.H. Jørgensen, T. Rami, S. Israr, G. Fontana, M. de Knegt, A. Fuchs, P. Lyden, A. Trento, D.L. Bhatt, M.B. Leon, R.R. Makkar, D. Ramzy, W. Cheng, R.J. Siegel, L.M. Thomson, G. Mangat, B. Hariri, F.J. Sawaya, H.K. Iversen, Subclinical leaflet thrombosis in surgical and transcatheter bioprosthetic aortic valves: an observational study, Lancet 389 (2017) 2383–2392, http://dx.doi.org/10.1016/S0140-6736(17)30757-2.

[38] A.C. Egbe, S.V. Pislaru, P.A. Pellikka, J.T. Poterucha, H.V. Schaff, J.J. Maleszewski, H.M. Connolly, Bioprosthetic valve thrombosis versus structural failure, J. Am. College Cardiol. 66 (2015) 2285–2294, http://dx.doi.org/10.1016/j.jacc.2015.09.022.

[39] E.D. Marchena, J. Mesa, S. Pomenti, C.M. y Kall, X. Marincic, K. Yahagi, E. Ladich, R. Kutys, Y. Aga, M. Ragosta, A. Chawla, M.E. Ring, R. Virmani, Thrombus formation following transcatheter aortic valve replacement, JACC: Cardiovasc. Intervent. 8 (2015) 728–739, http://dx.doi.org/10.1016/j.jcin.2015.03.005.

[40] S. Khodaei, M. Abdelkhalek, N. Maftoon, A. Emadi, Z. Keshavarz-Motamed, Early detection of risk of neo-sinus blood stasis post-transcatheter aortic valve replacement using personalized hemodynamic analysis, Struct. Heart 7 (2023) 100180, http://dx.doi.org/10.1016/j.shj.2023.100180.

[41] B.L. Moore, L.P. Dasi, Coronary flow impacts aortic leaflet mechanics and aortic sinus hemodynamics, Ann. Biomed. Eng. 43 (2015) 2231–2241, http://dx.doi.org/10.1007/s10439-015-1260-4.